LADRC applied to variable speed micro-hydro plants: Experimental validation

Baoling Guo, Seddik Bacha, Mazen Alamir, Amgad Tarek Mohamed, Cédric Boudinet

Version of Record: https://www.sciencedirect.com/science/article/pii/S0967066119300218
Manuscript_c8ba491c8ec4d1d21cbb372445ff56f2

LADRC applied to variable speed micro-hydro plants: experimental validation

Baoling GUO[a], Seddik BACHA[a], Mazen ALAMIR[b], Amgad MOHAMED[b], Cédric BOUDINET[a]

[a] *Univ. Grenoble Alpes, CNRS, Grenoble INP*, G2Elab, F-38000 Grenoble, France.*
[b] *Univ. Grenoble Alpes, CNRS, Grenoble INP*, GIPSA-Lab, F-38400 Saint Martin D'Hères, France.*

Abstract

To track the maximum power of a hydraulic turbine, the rotational speed needs to be adapted to flow rates variations, enabling higher speed tracking demands. Moreover, a Variable Speed Micro-Hydro Plant (VS-MHP) is a complex nonlinear system affected by large uncertainties. Active Disturbance Rejection Control (ADRC) can estimate and compensate the total disturbances in real-time, achieving higher robustness. A Linear-ADRC (LADRC) with the torque compensation is implemented to the speed control loop of a VS-MHP, which is tested under a real-time power Hardware-In-the-Loop benchmark. Experimental results prove its advantages for VS-MHP applications.

Keywords: Micro-hydro plants, variable speed, disturbances, LADRC, torque observer, robustness

1. Introduction

Hydropower is widely used in the renewable energy context [1, 2, 3, 4, 5]. Limited to the capacity of the Power Electronics (PE), variable speed technique is mainly implemented to small- or micro- hydro plants, which are mostly based on the "Run-of-River" (RoR). The RoR scheme usually has a low head and high water flow rates, Kaplan or Semi-Kaplan turbines become the most attractive prime mover for their high efficiency under such conditions [1, 2]. The hydraulic efficiency of Kaplan-type turbine is sensitive to water flow rate variations and rotational speed changes, the variable speed operation can help find the best efficiency point when the hydraulic conditions change [4]. Besides, variable speed techniques can optimise the operation process by mitigating the cavitation effects [5], alleviating water hammer disturbances [2], and optimizing transient processes [6]. Thus, Variable Speed Micro-Hydro Plants (VS-MHP) equipped with PE units gives rise to advantages in the hydraulic context [1, 2, 3, 4, 5, 6]. In this paper, a VS-MHP of semi-Kaplan turbine coupled to a Permanent Magnet Synchronous Generator (PMSG) is considered. The hydropower generation system is connected to the power grids via back-to-back full PE converters.

The rotational speed of hydraulic turbine needs to be adapted to the water flow rates variations in order to achieve the Maximum Power Point Tracking (MPPT) in a VS-MHP, which enables higher speed tracking demands [2]. MPPT operation provides an optimal speed reference for the speed control loop. Then, Proportion-Integration (PI) controllers are commonly used for the speed regulation due to their simplified structure, high steady-state accuracy, and stability [7]. Nevertheless, a VS-MHP is a nonlinear system disturbed by various internal and external uncertainties [6]. Several internal disturbances must be considered: A PMSG is faced with various uncertainties such as parameters variations caused by the aging factor, the non-constant friction, and the nonlinear magnetic

☆* Institute of Engineering Univ. Grenoble Alpes
*Corresponding author: Baoling.Guo@g2elab.grenobble-inp.fr (Baoling GUO)

field effect [8]; Additionally, PE itself is full of uncertainties including non-constant parameters caused by the aging factor, nonlinear variations due to heat effects. External disturbances mainly involve the following aspects: The water dynamics inside the penstocks and the actuator's dynamics cause pressure head oscillations, which would result in torque fluctuations [9]. Also, there are cases where the turbine operates in unstable regions, being unavoidable and resulting in severe vibrations [10]. The nonlinear features and large unpredictable disturbances in VS-MHPs would negatively affect the speed control performance. The increasing demands for high robustness and unavoidable limitations of traditional PI controllers have driven the engineers to apply more efficient control solutions [6, 7, 8, 11, 12, 13, 14, 15].

Large advanced control techniques such as adaptive Proportion-Differentiation-Integration (PID) [7], Fuzzy control [11], sliding mode control [12], and Active Disturbance Rejection Control (ADRC) [6, 13, 14, 15] are proposed to improve the speed control performance. Due to high robustness and advantages of less depending on the knowledge of a plant model, ADRC is increasingly implemented to the speed control of electrical drive systems [6, 13, 14, 15]. The key module in the frame of ADRC is the Extended State Observer (ESO). The internal dynamics and external disturbances are lumped together as the generalized disturbances, which are defined as an extended state variable. Then, total disturbances are estimated via the ESO and actively compensated into the closed-loop dynamics in real-time, which achieves high robustness in dealing with uncertainties. Further, Linear-ADRC (LADRC) has been proposed in [16], which make the controller design and parameter tuning more practical. Large applications prove that it can achieve nearly the same performance as nonlinear ADRC with less complexity [8, 13, 16, 17, 18]. Moreover, the large hydraulic torque variations bring great estimation burden for ESO [6, 15], which would affect the speed tracking performance. If the torque information could be obtained and appropriately used, the estimation efficiency would be enhanced. However, a physical torque sensor is still expensive; some sensor-less approaches can observe the load torque precisely at the price of the extra computational complexity [15, 19]. A simple on-line torque identification approach discussed in [18] is employed in this design, which can track the hydraulic torque dynamics efficiently.

In this paper, a LADRC-based speed controller is designed to improve the speed tracking performance, thus achieving efficient MPPT operation. The key features of the proposed speed control strategy are as follow: 1) It achieves faster control dynamics and higher robustness against various external disturbances and internal uncertainties; 2) It introduces an on-line torque observer into the speed control loop, which enables more efficient ESO; 3) It is simple to design and tune the speed controller for practical engineers. This paper is organised as follows: In Section 2, the VS-MHP under study is modelled and described. In Section 3, a LADRC-based speed controller is designed, and a hydraulic torque observer is introduced to enhance the efficiency of ESO. In Section 4, the suggested LADRC-based speed controller is validated under a real-time power Hardware-In-the-Loop (HIL) benchmark. Conclusions are indicated in Section 5.

2. Variable speed micro-hydro plant

The VS-MHP under study includes three parts: Hydraulic turbine, PMSG, and Power Electronics interfaces, which are modelled and described in the following subsections. Besides, the employed MPPT technique and the control design of VS-MHP are explained before starting the LADRC-based speed controller design.

2.1. Mathematical model of hydraulic turbine

In this paper, a propeller-type semi-Kaplan turbine of fixed blades and fixed guide vanes is considered, which has a similar operating feature to wind turbines [20]. The available hydraulic power P_h (W) depends on the net water head $H(m)$ and the water flow rate Q (m^3/s):

$$P_h = \rho \cdot g \cdot H \cdot Q \tag{1}$$

where ρ (kg/m^3) is the density of water, g is the acceleration due to gravity (m/s^2).

Hydraulic turbine efficiency η strongly affects the net output mechanical power P_m (W) as follows:

$$P_m = \eta \cdot P_h \tag{2}$$

The hydraulic mechanical torque is represented by (3), and ω (rad/s) is the hydraulic turbine rotational speed.

$$T_m = \frac{P_m}{\omega} \tag{3}$$

The steady-state efficiency of the semi-Kaplan hydraulic turbine is experimentally described in [3], which is approximated by the following expressions:

$$\eta(\lambda, Q) = \frac{1}{2}[(\frac{90}{\lambda_i} + Q + 0.78)exp(\frac{-50}{\lambda_i})]3.33Q \tag{4}$$

where λ_i is given by

$$\lambda_i = [\frac{1}{\lambda + 0.089} - 0.035]^{-1} \tag{5}$$

where $\lambda = RA\omega/Q$, R (m) is the radius of the hydraulic turbine, A (m^2) is the area swept by rotor blades.

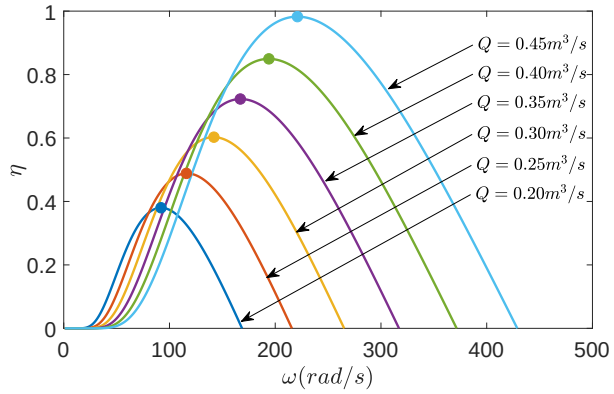

(a) Efficiency versus rotational speed

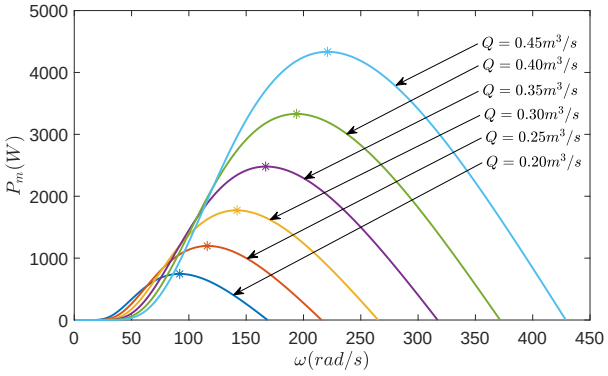

(b) Power versus rotational speed

Figure 1: Variable speed Semi-kaplan turbine model, with fixed head of $H = 1m$, $R = 0.25m$

The efficiency described by (4) and the generating hydraulic power curves (2) are shown in Figure 1. The figures indicate that when water flow rates change, there exists an optimal rotational speed that maximizing the efficiency.

2.2. Mathematical model of PMSG

In the synchronous dq frame, the PMSG can be modelled as follows:

$$\begin{aligned} v_d &= L_d \frac{di_d}{dt} + R_s i_d - \omega_e L_q i_q \\ v_q &= L_q \frac{di_q}{dt} + R_s i_q + \omega_e (L_d i_d + \psi_f) \end{aligned} \tag{6}$$

where v_d and v_q are the stator voltage vector of q-axis and d-axis, respectively; i_d and i_q are the stator current vector of q-axis and d-axis, respectively; L_d and L_q are the inductance of stator winding of q-axis and d-axis, respectively; R_s is the stator winding resistance; ψ_f is the permanent magnet flux vector, ω_e is the electrical rotational speed.

Electromagnetic torque T_e in the dq coordinate system is given by (7), where n_p is the number of pole pairs.

$$T_e = \frac{3}{2} n_p (\psi_f i_q + (L_d - L_q) i_q i_d) \tag{7}$$

If $L_d = L_q$ or $i_d = 0$, the expression (7) is simplified by

$$T_e = \frac{3}{2} P_n \psi_f i_q \tag{8}$$

A mechanical dynamic model between hydraulic turbine and PMSG is expressed by

$$J \frac{d\omega}{dt} = T_e - T_m - B\omega \tag{9}$$

where J is the total inertia; B is the friction factor; T_m is the hydraulic driven torque.

2.3. Adaptive Perturb and Observe MPPT technique

Perturb and Observe (P&O) MPPT technique does not require the prior knowledge of the system or additional flow rate sensors. Such advantages make it preferable for VS-MHPs because it is not easy to measure flow rates exactly in real-time. The converter and generator losses can change the maximum power point location of the whole hydropower system [20]. Therefore, when the shaft speed is perturbed, the injected power to the grid is observed (but not the mechanical power of hydraulic turbine) [20]. The grid power and the speed variations are computed respectively by

$$\begin{aligned} \Delta P_g &= P_g(k) - P_g(k-1) \\ \Delta\omega &= \omega(k) - \omega(k-1) \end{aligned} \tag{10}$$

The perturbing direction for hydro turbine rotational speed is determined by $\delta(t) = sgn(\Delta P_g) sgn(\Delta\omega)$. If $\delta(t)$ is positive, the speed increases in order to make the system track towards the maximum power point; otherwise, the speed decreases [2]. However, the speed tracking dynamics and oscillations appearing in the steady state highly depend on the perturbing coefficient K and the sampling time T_e. To address the trade-off issue between steady oscillations and its tracking speed, an adaptive perturbing coefficient K_{adap} is thus employed in [2]. The speed reference is updated by

$$\omega^*(k) = \omega(k) + \int_{t_{k-1}}^{t_{k-1}+T_e} K_{adap} \delta(t) dt \tag{11}$$

Finally, the output of the MPPT provides the optimal speed reference for the speed control loop.

2.4. Control of variable speed micro-hydro plant

The power architecture of VS-MHP with its control design is schematically presented in Figure 2. The PMSG is driven by a semi-Kaplan hydraulic turbine, and the full back-to-back PE converters are employed to transfer the hydraulic power as much as possible to the grid.

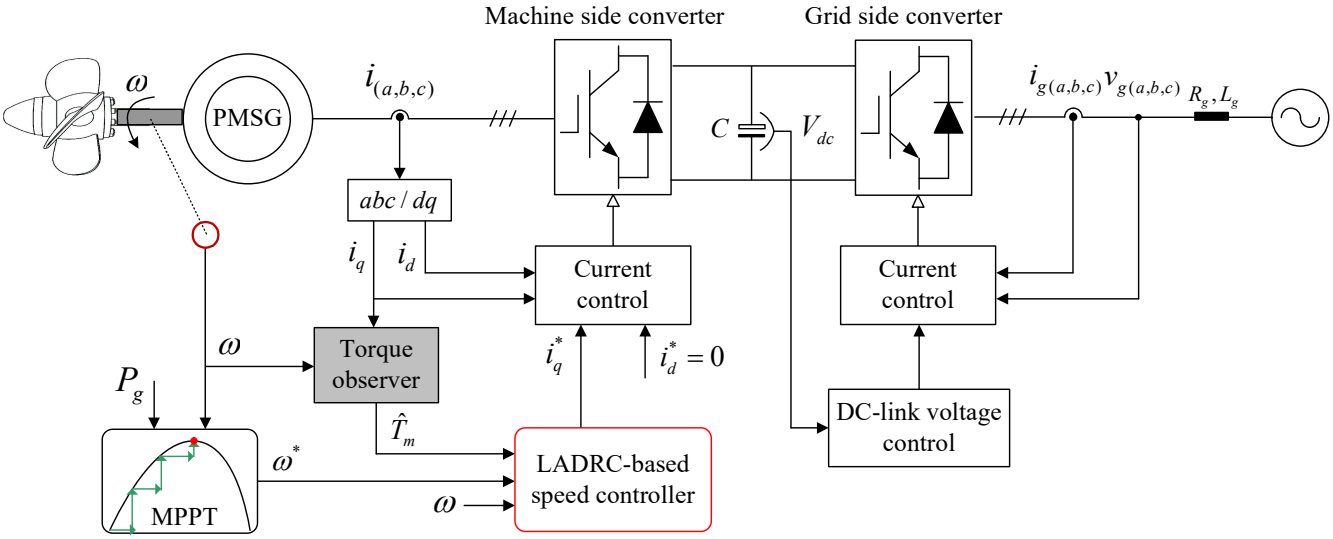

Figure 2: Power architecture of VS-MHP and its global control design, where $i_{(abc)}$ represents the components of the machine current vector, $\hat{T}_m$ is the estimated hydraulic torque, V_{dc} is the DC-link voltage, $i_{g(abc)}$ represents the components of the grid current vector, $v_{g(abc)}$ represents the components of the grid voltage vector, L_g and R_g are the inductance and resistance of the grid filter, respectively.

The machine-side converter control consists of two cascaded control loops. Usually, the external speed control loop regulates the turbine shaft to run at an optimal rotational speed [2]. As aforementioned, an adaptive MPPT technique is employed to generate the optimal speed reference. The rotational speed is determined by the dynamic function of the hydraulic torque and the machine electromagnetic torque. The machine torque is controlled through the stator current vector control upon a rotating dq synchronous reference frame. PI controllers are applied into the d-axis and q-axis current control loops, respectively. Further, a LADRC-based speed control with torque compensation is employed, it offers a fast dynamic response and high robustness under various disturbed conditions, which will be discussed in Section 3.

The grid-side converter control includes double closed control loops. The outer DC-link voltage loop ensures the stability of DC bus voltage. The inner loop needs to control the current to synchronize with the grid, achieving high quality injected current.

3. LADRC-based speed control strategy

The dual-loop control design of machine-side converter is presented in Figure 3. A first-order LADRC-based speed controller is introduced to improve the speed tracking performance, thus achieving efficient MPPT operation. ESO can estimate external disturbances and internal dynamics in real-time. A proportional gain is employed to regulate the rotational speed. Note that the P&O MPPT operation imposes a speed tracking process before it

reaches the maximum power point, which behaves like a transient process. The overshoot caused by the set-point input is mitigated, so the transient profile is neglected in this design.

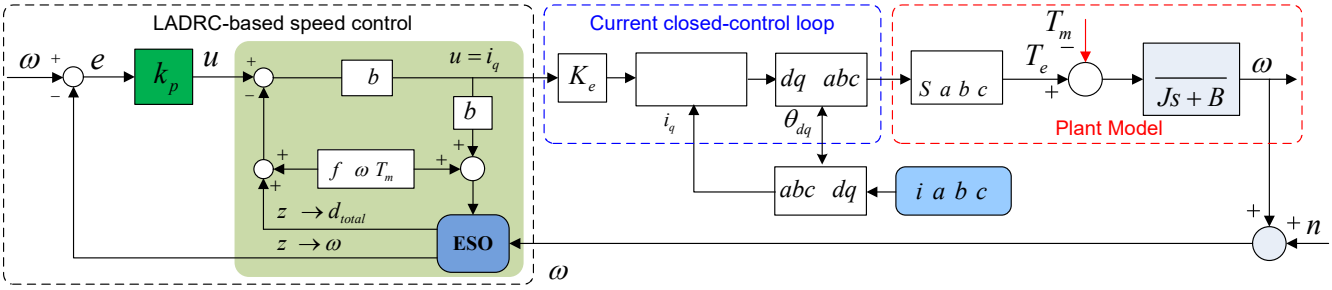

Figure 3: Dual-loop control design of machine-side converter, $K_e = \frac{3}{2} n_p \psi_f$ the torque constant, n the measurement noises

3.1. Canonical form

Before applying the LADRC paradigm, a key procedure is to reformulate a practical control issue to the canonical mode of cascade integrators as the expression (12). A systematic design procedure for a class of ADRC-based control applications is detailed in [14, 16, 21], which can be followed for the rotational speed control design.

$$\begin{cases} \dot{x}_1 = x_2 \\ \vdots \\ \dot{x}_2 = x_3 \\ \dot{x}_{n-1} = x_n \\ \dot{x}_n = bu + f_0(x_1, x_2, \cdots, x_n) + f_1(x_1, x_2, \cdots, x_n, w(t), t) \\ \dot{x}_{n+1} = h \\ y = x_1 \end{cases} \tag{12}$$

where $x_1, x_2, \cdots, x_n$ are the state variables, y is the output, u is the control input, $w(t)$ is the uncertain external disturbance, b is the control gain, $f_0(x_1, x_2, \cdots, x_n)$ represents the known disturbances, $x_{n+1} = f_1(x_1, x_2 \cdots, x_n, w(t), t)$ represents the unknown disturbances, which is defined as an extended stated, and $h = \dot{f}_1(x_1, x_2 \cdots, x_n, w(t), t)$ is the time derivative of disturbances [21].

By simply manipulating expressions (8) and (9), the dynamic model can be rewritten by

$$\frac{d\omega}{dt} = \frac{3}{2J} n_p \psi_f i_q^* - \frac{T_m}{J} - \frac{B\omega}{J} \tag{13}$$

Firstly, it is essential to choose the output y to be controlled and the input u to be manipulated. Based on (13), ω is defined as the output y, i_q^* is chosen as the input u.

Then, the order of LADRC-based controller is chosen according to the order of the plant model. A first-order LADRC is hence considered, and a second-order ESO is needed.

Further, a crucial step is how to reformulate the problem by lumping various known, unknown components into the total disturbances. The efficiency of LADRC largely depends on its key element ESO, and the accuracy of ESO is affected by the total disturbances [21]. Expression (13) indicates that speed variations and hydraulic torque fluctuations are the main external disturbances for the speed control loop. To mitigate the effects of large speed changes, $-B\hat{\omega}/J$ is easy to be computed as the known disturbances, where $\hat{\omega}$ can be estimated by ESO. In fact, the hydraulic torque fluctuations are the main external disturbances. The hydraulic torque information is needed to mitigate the effects of torque variations. While a physical torque sensor is expensive, an on-line torque identification approach based on the mechanical dynamic equation (9) is thus employed, which is detailed in the following part.

Now, let $y = x_1 = \omega$, $u = i_q^*$, $b_0 = \dfrac{3}{2J} n_p \psi_f$, $x_2 = d_{total}$ is defined as an extended state variable, the time derivative of disturbances is given by $\dot{x}_2 = h$. The speed control problem is formulated to a first-order standard model by (14), having the same form to (12).

$$\begin{cases} \dot{x_1} = b_0 u + + f_0(\hat{\omega}, \hat{T}_m) + d_{total} \\ \dot{x_2} = h \\ y = x_1 \end{cases} \tag{14}$$

where d_{total} can be represented by (15). It implies that, if $\hat{T}_m$ is well observed by the torque observer, the total disturbances estimated by ESO are very small.

$$d_{total}(t) = (b - b_0) i_q^* - (\frac{T_m}{J} + \frac{B\omega}{J}) + (\frac{\hat{T}_m}{J} + \frac{B\hat{\omega}}{J}) + w(t) \tag{15}$$

3.2. Extended State Observer

Based on the canonical model (14), a second-order ESO is constructed as follows:

$$\begin{cases} \dot{z}_1 = -\beta_1(z_1 - \omega) + b_0 i_q^* + z_2 + f_0(\hat{\omega}, \hat{T}_m) \\ \dot{z}_2 = -\beta_2(z_1 - \omega) \end{cases} \tag{16}$$

where z_1, z_2 are the estimations of the output ω and the unknown disturbances d_{total}, respectively; the positive gains $\beta_1 = 2\omega_0$ and $\beta_2 = \omega_0^2$ are chosen such that characteristic polynomial (17) is Hurwitz stable , and ω_0 represents the bandwidth of ESO [16].

$$\lambda(s) = s^2 + \beta_1 s + \beta_1 2 = (s + \omega_0)^2 \tag{17}$$

3.3. Control law design

The estimated disturbances z_2 and the known disturbances $f_0(\hat{\omega}, \hat{T}_m)$ are both compensated in the feedback control channel, the feedback control law is represented by

$$i_q^* = \frac{k_p(\omega^* - z_1) - [z_2 + f_0(\hat{\omega}, \hat{T}_m)]}{b_0} \tag{18}$$

where k_p is the proportional gain of controller.

Within the ESO's bandwidth, the unknown disturbance is well estimated ($z_2 \approx d_{total}$), the original disturbed plant model $G_p(s)$ is modified to be an integrator as follows [22]:

$$\hat{G}_p(s) = \frac{y(s)}{u_0(s)} \approx \frac{1}{s} \tag{19}$$

Thus, a zero steady-state error for the speed can be achieved by employing a proportional controller. The closed-loop transfer function of the speed control loop is approximately represented by

$$H_c(s) \approx \frac{k_p \frac{1}{s}}{1 + k_p \frac{1}{s}} = \frac{1}{1 + \frac{s}{k_p}} \tag{20}$$

where the closed-loop bandwidth of controller $\omega_c \approx k_p$.

3.4. Parameter tuning

Being different from a PI-type controller, LADRC-based controller is a Two-Degree-Of-Freedom (2DOF) controller, ω_c and ω_0 can be adjusted independently [23]. Theoretically, the bigger the bandwidth, the faster the disturbance is observed and rejected by the controller [16]. However, in a real application into a VS-MHP, the bandwidth is limited by sensor noises and practical considerations. An optimal bandwidth can be tuned under a real physical experimental benchmark, where the performance is maximized subject to its physical constraints [17]. The tuning process is as follows:

- Firstly, ω_c and ω_0 are designed to ensure the stability of the control system, and tested under the software environment. Generally, ω_c is chosen to ensure the fast enough transient response, such as the setting time requirements [16]. The bandwidth ω_0 is normally set to be 5-10 times of the controller's bandwidth ω_c;
- Then, the control parameters are retuned and validated under the real-time physical experiments. The tests start with small values that can meet the basic performance requirements;
- Further, both of them are incrementally increased until the control signal exceeds the noise tolerance of the q-axis current reference;
- Finally, ω_c and ω_0 are increased or decreased individually to find a best speed tracking performance.

In addition, PI-controller with the same bandwidth is designed to provide an equal comparison with the LADRC-based speed control. Details about adaptive MPPT design and PI-controller design can refer the work in [2, 24]. Well-tuned control parameters are given in Table 1.

3.5. Hydraulic torque observer

The previous discussion in Section 3 suggests that the hydraulic torque information is essentially needed for an efficient LADRC-based speed controller, thus an on-line torque observer is employed in this design. By taking use of the information of i_q and ω, the torque can be identified based on the following expression:

$$T_m = K_e i_q - B\omega - J\dot{\omega} \tag{21}$$

where $K_e = \frac{3}{2} n_p \psi_f$ is the torque constant.

To attenuate the negative effects from measurements noises, a low pass filter $\frac{1}{T_0 s+1}$ is applied to the output side, then Laplace transformation is conducted to obtain the transfer function as follows:

$$\hat{T}_m(s) = [K_e i_q(s) - B\omega(s) - Js\omega(s)] \frac{1}{T_0 s + 1} \tag{22}$$

The expression (22) can be manipulated as follows:

$$\begin{aligned} \hat{T}_m(s) &= \frac{K_e i_q(s) - B\omega(s) + \frac{J}{T_0}\omega(s) - Js\omega(s) - \frac{J}{T_0}\omega(s)}{T_0 s + 1} \\ &= \frac{K_e i_q(s) - B'\omega(s)}{T_0 s + 1} - \frac{J}{T_0}\omega(s) \\ &= \omega_1(s) - \frac{J}{T_0}\omega(s) \end{aligned} \tag{23}$$

where $B' = B - \frac{J}{T_0}$, $\omega_1(s) = \frac{K_e i_q(s) - B'\omega(s)}{T_0 s+1}$.

An inverse Laplace transformation is applied to get the time domain representation (24). The complete observer design diagram is schematically illustrated in Figure 4.

$$\hat{T}_m = \omega_1 - \frac{J}{T_0}\omega \tag{24}$$

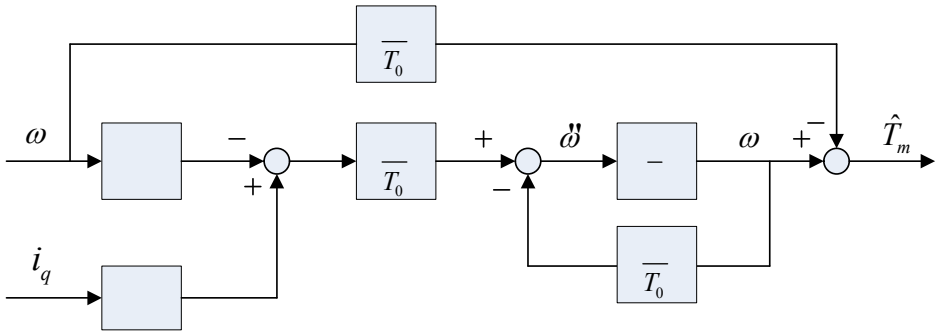

Figure 4: Schematic of the hydraulic torque observer

Finally, the control design of the machine-side converter is presented in Figure 5. This paper is dedicated to the machine-side speed control, so the control diagram of grid-side converter is not described here.

4. Experimental validation

The experiments have been performed inside the real-time power HIL platform [25, 26], which has been adapted for variable speed hydraulic tests as shown in Figure 6. Due to high costs and uncertain testing conditions of a real physical micro-hydro plant, a reduced-scale physical hydraulic simulator is developed in the laboratory. The hydro turbine model is implemented in the dSPACE hardware (DS1005), and its efficiency and water flow rates versus the rotational speed for different valve values are stored in the look-up tables. Then, the physical simulation

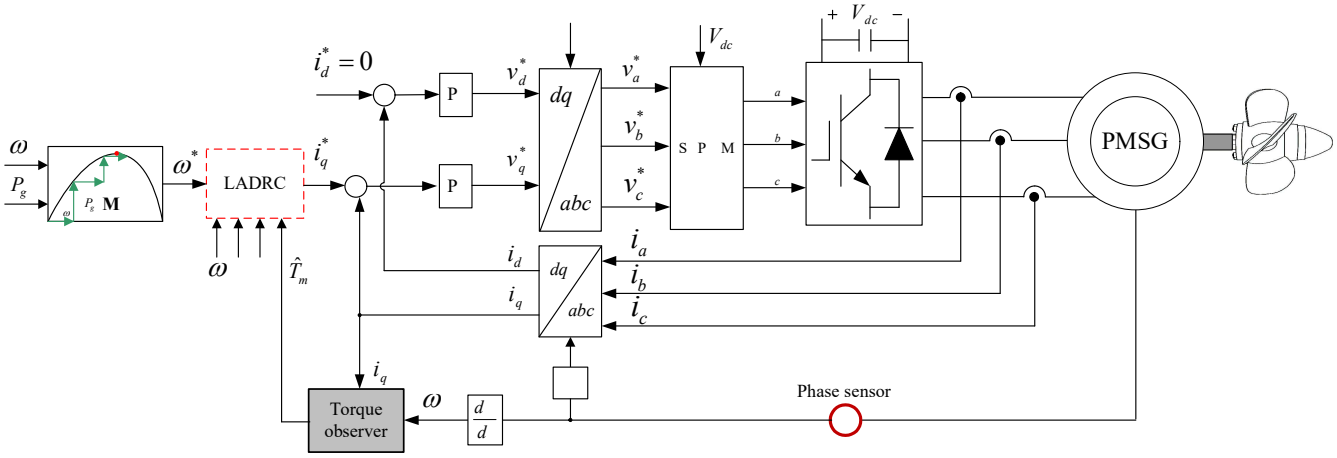

Figure 5: Control design of machine-side converter, where θ_e is the electrical angle phase, v_a^*, v_b^*, v_c^* are the machine voltages references, S_a, S_b, S_c are the switching signals, SVPWM: Space Vector Pulse Width Modulation.

of the hydraulic turbine is achieved by a torque-controlled Direct Current Motor (DCM). The DCM control is implemented into a TMS320F240 digital signal processor. Finally, the PMSG is directly driven by the DCM, and the generator is connected to the power grid via back-to-back voltage sources converters. The control algorithms of VS-MHP are conducted with the same dSPACE hardware under MATLAB/Simulink environment. Parameters of the testing benchmark are listed in Table 1.

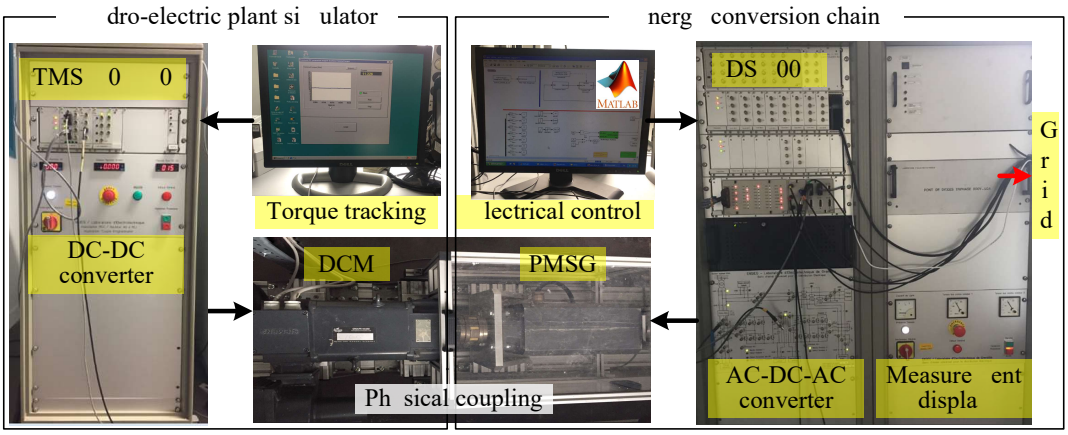

Figure 6: Real-time HIL-based VS-MHP experimental benchmark

4.1. Torque observer validation

Firstly, experiments are carried out to verify the effectiveness of the torque identification approach. Different types of torque disturbances are considered. In Figure 7 (a), the torque tracking performance of the starting process is presented. In Figure 7 (b), a step-up torque of $3N.m$ is first added and then it steps back to the original value. Further, torque oscillations happen due to pressure head oscillations, a cycle oscillated torque is added to the basis torque as shown in Figure 7 (c). The numerical model of oscillated torque is described in the following part.

The torque oscillations result from the water dynamics inside the penstocks and the actuator's dynamics [9]. The numerical model of torque oscillations is given by equations (25a)-(25g) [9]. The mathematical models of the water dynamics inside the penstocks are given by equations (25c)-(25d). The dynamic actuator considered

Table 1: Parameters of the experiment benchmark

Parameters of experimental benchmark			
Parameters	Values	Parameters	Values
Rated power	6 kW	Pole pairs	4
Magnet flux ψ_f	0.11 Wb	Total inertia	$0.03 Kg.m^2$
Armature R_s	0.17 Ω	Friction factor	0.01 $N.m.s$
d-axis L_q	0.0017 H	Switch frequency	10 kHz
q-axis L_d	0.0019 H	DC-link voltage	400 V
Speed control parameters			
Adaptive MPPT		PI-controller	LADRC-based controller
$K_{min} = 0.5$, $K_{max} = 2$, $T_e = 0.1s$		$k_p = 2.5$, $k_i = 333$	$\omega_c = 30$, $\omega_0 = 150$

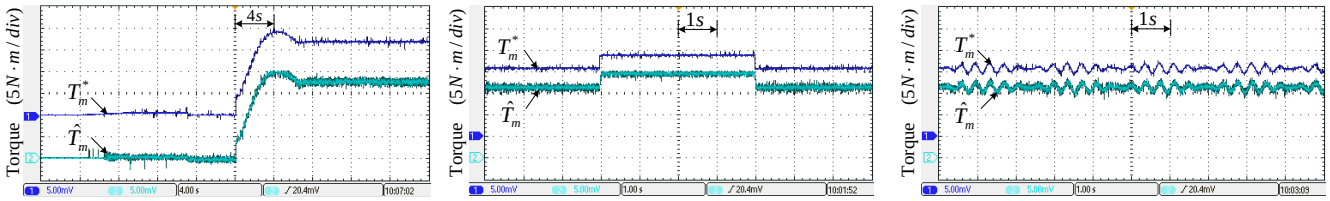

(a) Torque of soft starting process (b) Step hydraulic torque (c) Oscillated hydraulic torque

Figure 7: Torque observer performance under different types of hydraulic torque, T_m^* is the emulated torque reference

is modelled by a second-order differential equation given by equations (25e)-(25f). All parameters appearing in equations (25a)-(25g) are provided by the manufacturer, which are then scaled to the laboratory experimental level.

$$T_d(t) = D^3 H_n(t) \tilde{T}_{11}(N(t), H_n(t), \gamma(t)) \tag{25a}$$

$$Q(t) = D^2 \sqrt{H_n(t)} \tilde{Q}_{11}(N(t), H_n(t), \gamma(t)) \tag{25b}$$

$$H_n(t) = C_h x_h(t) \tag{25c}$$

$$x_h(t+\tau) = A_h x_h(t) + B_h Q(t) \tag{25d}$$

$$\gamma(t) = C_a x_a(t) \tag{25e}$$

$$x_a(t+\tau) = A_a x_a(t) + B_a \gamma_c(t) \tag{25f}$$

$$N(t+\tau) = N(t) + \frac{30\tau}{\pi J_t} T_d(t) \tag{25g}$$

where the different parameters of the model given by equations (25a)-(25g) are defined in Table 2.

Table 2: The definitions of the hydraulic dynamic variables

T_d	Oscillated hydraulic torque $(N.m)$	x_h	Internal states of the penstocks
D	Turbine's diameter (m)	x_a	Actuator's internal states
H_n	Net pressure head (m)	γ	Turbine's guide vanes opening $(ratio)$
$\tilde{T}_{11}$	Regression model of the torque Hill charts	γ_c	Guide vanes angle set-point $(ratio)$
N	Turbine's rotational speed (rpm)	J_t	Turbine's moment of inertia $(Kg.m^2)$
Q	Water flow rate at the side of the turbine m^3/s	A_h, B_h, C_h	Parameters of the penstocks model
$\tilde{Q}_{11}$	Regression model of the flow rate Hill charts	A_a, B_a, C_a	Parameters of the actuator model

Experimental results in Figure 7 show that the torque observer is efficient to observe torque dynamics of the starting process, variations of step-up or step-down torque, and the cycle oscillated torque.

4.2. Variable speed control validation

To verify the speed tracking performance of LADRC-based controller, comparative experiments between strategies with torque compensation and without torque compensation have been conducted. To start the VS-MHP smoothly, a soft starting process is employed as shown in Figure 8. Firstly, a small initial torque is used to overcome the friction torque, the speed increases slowly; Then, the controller starts working under speed controlled mode in a no-load state; Finally, the MPPT mode is enabled and the rotational speed adapts to water flow rate variations. The results suggest that the overshoot of rotational speed is reduced with torque compensation, the total disturbances estimated z_2 is nearly zero, raising advantages when the torque is varying sharply.

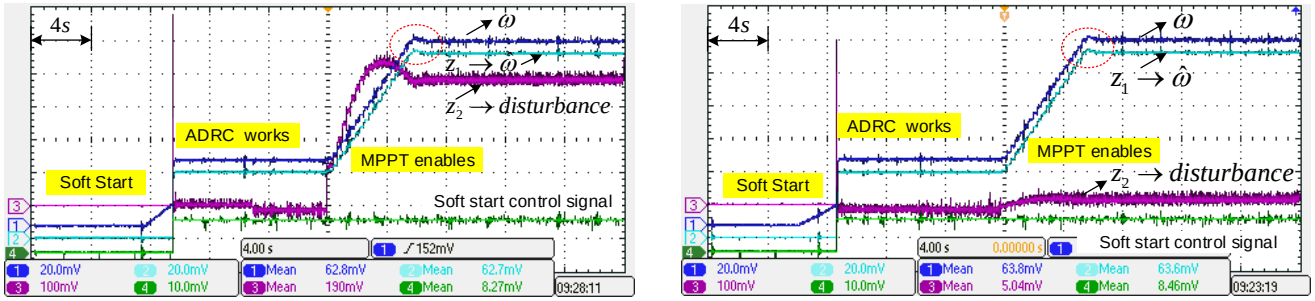

(a) LADRC without torque compensation (b) LADRC with torque compensation

Figure 8: Starting process of the VS-MHP, with ω the rotational speed ($20rad/s/div$), z_1 the estimation of the rotational speed ($20rad/s/div$), z_2 the estimation of total unknown disturbances ($100/div$)

Figure 9 shows the MPPT process under water flow rate variations of $Q = [300l/s, 320l/s, 340l/s, 320l/s, 300l/s]$. With LADRC-based speed controller, the system always tracks the optimal rotational speed efficiently. Moreover, experiments results indicate that the speed tracking performance is improved by compensating the time-varying torque, particularly at the point when water flow rates vary fast.

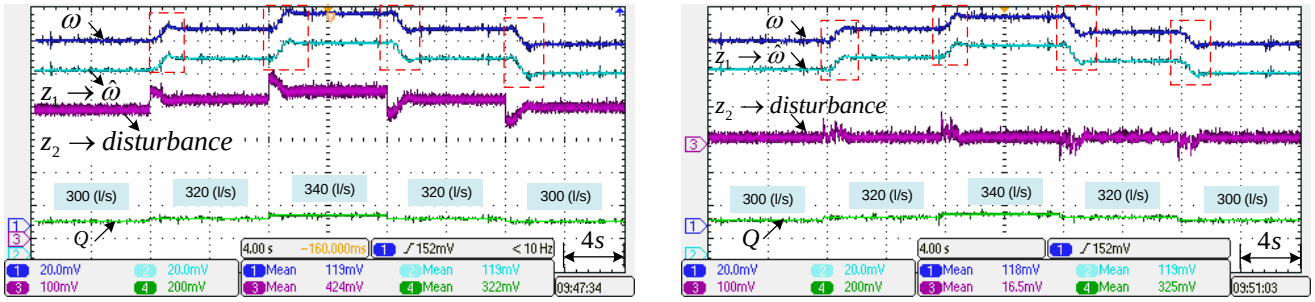

(a) LADRC without torque compensation (b) LADRC with torque compensation

Figure 9: MPPT performance when water flow rates vary, with ω the rotational speed ($20rad/s/div$), z_1 the estimation of rotational speed ($20rad/s/div$), z_2 the estimation of total unknown disturbances ($100/div$)

4.3. Robustness test

Robustness tests are carried out considering both external disturbances caused by disturbed torques and internal uncertainties due to time-varying plant parameters.

4.3.1. External disturbances test

Different types of disturbed torques are tested in this part. Comparative experimental results of PI controller, LADRC without torque observer, and LADRC with torque observer are provided in Figure 10. In cases (a) and (b), a step-up and step-down torque disturbance of $3N.m$ are added to the hydraulic turbine torque, respectively. Compared with the PI controller, LADRC-based controllers can reduce the speed undershoot/overshoot due to the step torque disturbances, and the control dynamics are significantly increased. Further, the robustness and disturbance rejection ability are enhanced by introducing the torque observer. In case (c), the oscillated torque T_d provided in Subsection 4.1 is added to the basis torque T_m. The speed variations caused by torque oscillations are significantly smoothed with the LADRC-based controller, and the LADRC with the torque observer has the best performance.

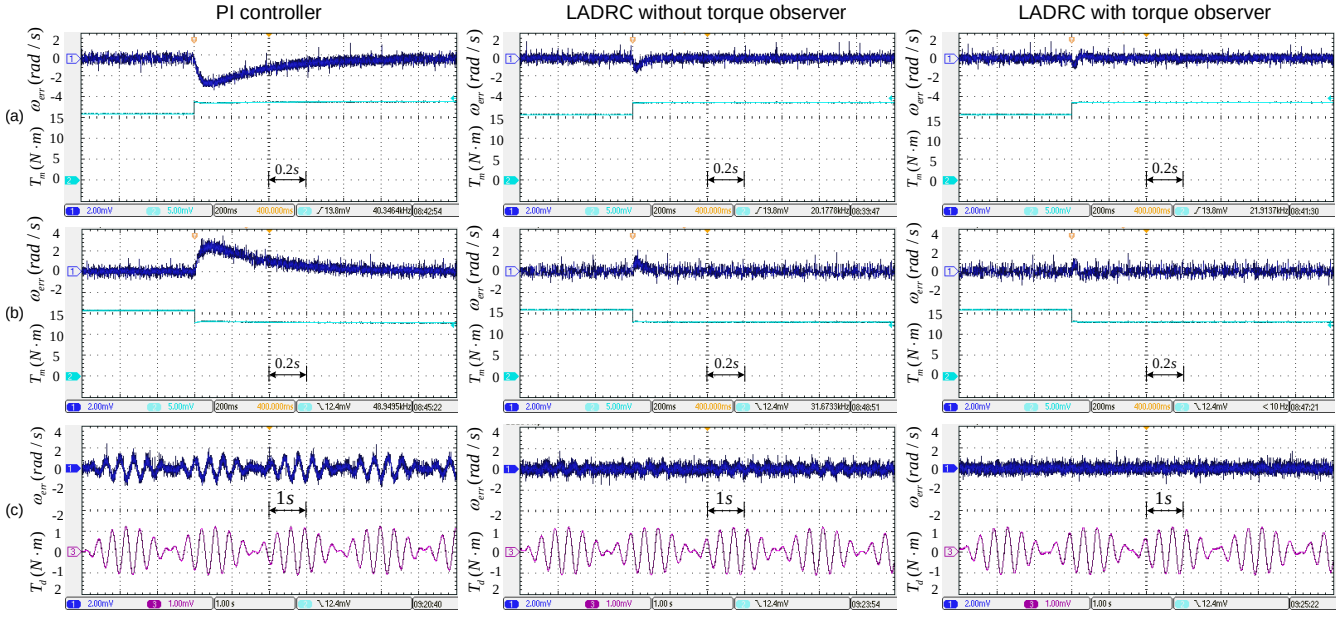

Figure 10: Robustness of speed control under torque disturbances: (a) Step-up torque disturbance, (b) Step-down torque disturbance, (c) Oscillated torque disturbance, with $\omega_{err} = \omega - \omega^*$

4.3.2. Internal uncertainties test

The total inertia of VS-MHP can be expressed by $J = J_{PMSG} + J_{hdy}$, J_{PMSG} is the inertia of the PMSG, and J_{hdy} is the inertia of the hydraulic turbine. These two inertia values would vary when hydraulic conditions change [8]. Suppose that the knowledge of system inertia is not precise, the controller is designed with different inertia values, but tested in the same benchmark. Figure 11 shows the speed tracking responses under different inertia values. It is expected that the increased inertia degrades the speed tracking performance, however, even the inertia value is increased to be 4 times of the normal value, the speed tracking process is stable and still under the toleration. The proposed LADRC-based speed control achieves high robustness in the presence of inertia variations.

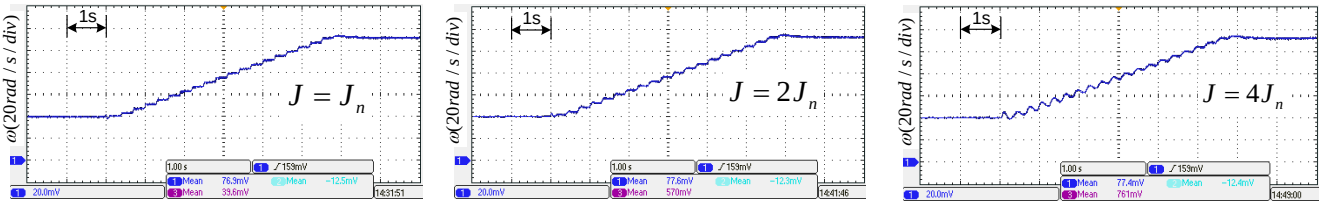

(a) J = Jn (b) J = 2Jn (c) J = 4Jn

Figure 11: Performance comparisons under different inertia values

5. Conclusions

In this paper, a VS-MHP of semi-Kaplan turbine coupled to a PMSG is studied. The hydropower generation system is connected to the power grids via back-to-back full PE converters. A VS-MHP is a classical nonlinear system disturbed by large uncertainties. ADRC-based controllers can estimate and compensate the influences of internal and external disturbances in real-time, which achieves high robustness and fast control dynamics. Thus, a LADRC-based speed controller is designed to improve the speed tracking performance, enabling efficient MPPT operation. To mitigate the negative effects caused by hydraulic torque variations, a torque observer is incorporated into the speed-control loop.

Different operation schemes are experimentally validated under a real-time power HIL benchmark. Some conclusions can be indicated: Firstly, the on-line torque observer can efficiently observe various torque disturbances such as torque dynamics of the starting process, step variations, and cycle oscillated torques. Further, the rotational speed can fastly track the speed reference during the starting process and the MPPT mode as well. The speed overshoot is reduced by compensating the hydraulic torque, particularly at the point when water flow rates vary. Robustness tests are carried out considering external disturbances and internal dynamics as well. Compared with PI-controllers, the proposed LADRC-based speed controller achieves higher robustness and faster dynamics in the presence of various torque disturbances and system inertia variations. Further, the disturbance rejection ability of speed control is improved by introducing the torque observer. Experimental results prove its advantages for VS-MHP applications.

Acknowledgement

This paper is supported by PSPC Innov'hydro project, which specifically brings together GE (General Electric) Renewable, EDF (Electricity of France), Grenoble INP and other key players in the hydroelectric sector, in France.

References

[1] A. Ansel, B. Robyns, Modelling and simulation of an autonomous variable speed micro hydropower station, Mathematics and Computers in Simulation 71 (4) (2006) 320 – 332, modeling and Simulation of Electric Machines, Converters and Systems. doi:https://doi.org/10.1016/j.matcom.2006.02.011.
URL http://www.sciencedirect.com/science/article/pii/S0378475406000498

[2] L. Belhadji, S. Bacha, I. Munteanu, A. Rumeau, D. Roye, Adaptive MPPT Applied to Variable-Speed Micro-hydropower Plant, IEEE Transactions on Energy Conversion 28 (1) (2013) 34–43. doi:10.1109/TEC.2012.2220776.

[3] J. Márquez, M. Molina, J. Pacas, Dynamic modeling, simulation and control design of an advanced micro-hydro power plant for distributed generation applications, International Journal of Hydrogen Energy 35 (11) (2010) 5772 – 5777, 3rd Argentinean and 2nd Latin American Congress inHydrogen and Sustainable Energy Sources. doi:https://doi.org/10.1016/j.ijhydene.2010.02.100.
URL http://www.sciencedirect.com/science/article/pii/S0360319910004003

[4] B. Guo, S. Bacha, M. Alamir, A. T. Mohamed, Variable speed micro-hydro power generation system: Review and Experimental results *, in: Symposium de Génie Electrique, Nancy, France, 2018.
URL https://hal.archives-ouvertes.fr/hal-01907850

[5] M. Valavi, A. Nysveen, Variable-speed operation of hydropower plants: Past, present, and future, in: 2016 XXII International Conference on Electrical Machines (ICEM), 2016, pp. 640–646. doi:10.1109/ICELMACH.2016.7732593.

[6] B. Guo, S. Bacha, M. Alamir, H. Imanein, An anti-disturbance ADRC based MPPT for variable speed micro-hydropower plant, in: IECON 2017 - 43rd Annual Conference of the IEEE Industrial Electronics Society, 2017, pp. 1783–1789. doi:10.1109/IECON.2017.8216302.

[7] J. Jung, V. Q. Leu, T. D. Do, E. Kim, H. H. Choi, Adaptive PID Speed Control Design for Permanent Magnet Synchronous Motor Drives, IEEE Transactions on Power Electronics 30 (2) (2015) 900–908. doi:10.1109/TPEL.2014.2311462.

[8] S. Li, Z. Liu, Adaptive speed control for permanent-magnet synchronous motor system with variations of load inertia, IEEE Transactions on Industrial Electronics 56 (8) (2009) 3050–3059. doi:10.1109/TIE.2009.2024655.

[9] H. Mesnage, Modélisation et contrôle avancé pour les centrales de turbinage de moyenne et haute chute, Ph.D. thesis, Université Grenoble Alpes (UGA) (2017).
URL http://www.theses.fr/2017GREAT025

[10] H. Mesnage, M. Alamir, N. Perrissin-Fabert, Q. Alloin, S. Bacha, Hydraulic-turbine start-up with "s-shaped" characteristic, in: Control Conference (ECC), 2015 European, IEEE, 2015, pp. 2328–2333.

[11] Y. Kung, M. Tsai, FPGA-Based Speed Control IC for PMSM Drive With Adaptive Fuzzy Control, IEEE Transactions on Power Electronics 22 (6) (2007) 2476–2486. doi:10.1109/TPEL.2007.909185.

[12] S. E. B. Elghali, M. E. H. Benbouzid, T. Ahmed-Ali, J. F. Charpentier, High-order sliding mode control of a marine current turbine driven doubly-fed induction generator, IEEE Journal of Oceanic Engineering 35 (2) (2010) 402–411. doi:10.1109/JOE.2010.2040402.

[13] S. Li, J. Li, Output predictor-based active disturbance rejection control for a wind energy conversion system with pmsg, IEEE Access 5 (2017) 5205–5214. doi:10.1109/ACCESS.2017.2681697.

[14] B. Guo, S. Bacha, M. Alamir, A review on ADRC based PMSM control designs, in: IECON 2017 - 43rd Annual Conference of the IEEE Industrial Electronics Society, 2017, pp. 1747–1753. doi:10.1109/IECON.2017.8216296.

[15] Z. Tong, G. Hong, X. Jinquan, K. Xiaolin, Q. Hao, Research on PMSM active disturbance rejection controller based on model compensation, in: 2015 18th International Conference on Electrical Machines and Systems (ICEMS), 2015, pp. 1593–1596. doi:10.1109/ICEMS.2015.7385295.

[16] Z. Gao, Scaling and bandwidth-parameterization based controller tuning, in: Proceedings of the American control conference, Vol. 6, 2006, pp. 4989–4996.

[17] B. Sun, Z. Gao, A DSP-based active disturbance rejection control design for a 1-kW H-bridge DC-DC power converter, IEEE Transactions on Industrial Electronics 52 (5) (2005) 1271–1277. doi:10.1109/TIE.2005.855679.

[18] Z. Liu, S. Li, Active disturbance rejection controller based on permanent magnetic synchronous motor model identification and compensation, Proceedings of the CSEE 28 (24) (2008) 118–123 (In Chinese).

[19] Z. Zedong, L. Yongdong, M. Fadel, X. Xi, A Rotor Speed and Load Torque Observer for PMSM Based on Extended Kalman Filter, in: 2006 IEEE International Conference on Industrial Technology, 2006, pp. 233–238. doi:10.1109/ICIT.2006.372295.

[20] H. Iman-Eini, D. Frey, S. Bacha, C. Boudinet, J.-L. Schanen, Evaluation of loss effect on optimum operation of variable speed micro-hydropower energy conversion systems, Renewable Energy 131 (2019) 1022 – 1034. doi:https://doi.org/10.1016/j.renene.2018.07.122.
URL http://www.sciencedirect.com/science/article/pii/S0960148118309194

[21] J. Han, From PID to active disturbance rejection control, IEEE transactions on Industrial Electronics 56 (3) (2009) 900–906.

[22] J. Tatsumi, Z. Gao, On the enhanced ADRC design with a low observer bandwidth, in: Proceedings of the 32nd Chinese Control Conference, 2013, pp. 297–302.

[23] R. Miklosovic, Z. Gao, A robust two-degree-of-freedom control design technique and its practical application, in: Conference Record of the 2004 IEEE Industry Applications Conference, 2004. 39th IAS Annual Meeting., Vol. 3, 2004, pp. 1495–1502 vol.3. doi:10.1109/IAS.2004.1348669.

[24] L. Belhadji, S. Bacha, D. Roye, Modeling and control of variable-speed micro-hydropower plant based on Axial-flow turbine and permanent magnet synchronous generator (MHPP-PMSG), in: IECON 2011 - 37th Annual Conference of the IEEE Industrial Electronics Society, 2011, pp. 896–901. doi:10.1109/IECON.2011.6119429.

[25] H. Gaztanaga, I. Etxeberria-Otadui, S. Bacha, D. Roye, Real-Time Analysis of the Control Structure and Management Functions of a Hybrid Microgrid System, in: IECON 2006 - 32nd Annual Conference on IEEE Industrial Electronics, 2006, pp. 5137–5142. doi:10.1109/IECON.2006.347976.

[26] I. Munteanu, A. I. Bratcu, S. Bacha, D. Roye, J. Guiraud, Hardware-in-the-loop-based simulator for a class of variable-speed wind energy conversion systems: Design and performance assessment, IEEE Transactions on Energy Conversion 25 (2) (2010) 564–576. doi:10.1109/TEC.2010.2042218.